UC Riverside
Other Recent Work

Title
ECEF Position Accuracy and Reliability: Inertial Navigation with GNSS Precise Point Positioning (PPP)

Permalink
https://escholarship.org/uc/item/4km0d6pz

Authors
Rahman, Farzana
Uwineza, Jean-Bernard
Farrell, Jay A.

Publication Date
2020-03-10

ECEF Position Accuracy and Reliability: Inertial Navigation with GNSS Precise Point Positioning (PPP)

Farzana Rahman, Jean-Bernard Uwineza, and Jay A. Farrell
{frimi, juwin001, farrell}@ee.ucr.edu.
Department of Electrical and Computer Engineering
University of California, Riverside, CA 92521

Abstract—**This report presents experimental results for a moving platform using GPS PPP data for state estimation. Results from two PPP GPS state estimation approaches are presented: point-wise least squares (LS) and aided inertial navigation (INS). The point-wise LS results provide information about the accuracy and reliability of PPP GPS information at each measurement epoch, independent of other epochs. The INS results show the performance that can be achieved by combining information across measurement epochs. INS results are included for two different grades of IMU: navigation grade and consumer grade.**

The report cites publications that contain more detailed explanations of the GNSS error sources, computation of PPP wide area correction, and the LS and aided INS estimation algorithms.

I. EXECUTIVE SUMMARY

Many connected and autonomous vehicles applications would benefit from navigation technologies that reliably achieve sub-meter position accuracy for moving platforms [1]. Real-time centimeter-level Earth-referenced positioning has been demonstrated using Global Navigation Satellite Systems (GNSS) system with local-area Differential-GNSS (DGNSS) approaches using dual frequency receivers [2]–[6] However multi-frequency receivers are currently expensive and implementation of local-area DGNSS approaches on a continental scale would be very expensive. Feasible implementations at continental or global scales are of interest for successful commercial automotive applications.

This research project studied the potential to use single-frequency GNSS receivers with Wide Area Differential GNSS (WADGNSS) such as Precise Point Positioning (PPP) to achieve performance exceeding the SAE J2945 specification (horizontal error 1.5 m and vertical error of 3 m at 68%) [7].

Phase A of this project presented a local differential correction computation methodology designed to be robust to latency and studied position estimation accuracy as a function of differential correction latency for stationary receivers [8]–[10]. The study showed that submeter accuracy at 95% probability was achievable when a sufficient number and diversity of satellites was available. This performance was robust to latency of up to 600 seconds.

Phase B of this project studied position accuracy as a function of differential correction latency for moving receivers using two navigation algorithms. Both algorithms incorporated the local differential correction approach defined in Phase A [8]. The Position, Velocity, Acceleration (PVA) approach used only DGNSS data with a Kalman filter (KF). The Inertial Navigation System (INS) approach used DGNSS and inertial measurement data within an extended Kalman filter (EKF). The study showed that DGPS PVA achieved 1 m horizontal accuracy at 90% and 2 m vertical accuracy at 95%, while the DGPS INS approach using a consumer-grade IMU achieved 1 m horizontal accuracy at 98% and 2 m vertical accuracy at 95% [11]. Both approaches achieved performance exceeding the SAE J2945 specification [7]. This performance was robust to correction communication latency of up to 500 seconds.

Phase C of the project investigated different WADGNSS approach, discussed sources of correction information, modeling agencies, and the existing data and model sources [12]. The report included a discussion about communication data requirements and a description of a PPP correction calculation algorithm suitable for communication via Sirius XM satellite channels. Finally, the report included, a PPP state estimation approach with experimental results for stationary receivers.

This report extends the PPP position estimation experimental results to a moving platform. This report includes short descriptions of different positioning algorithms (e.g. LS, INS) with pointers to references; discussion of data collection methods; and, performance analysis for the LS and INS algorithms for both navigation grade and consumer grade inertial sensors. The LS algorithm, which processes each epoch of data independently, would not be used in moving platform applications. It is only included as it facilitates analysis of the PPP GPS data accuracy at each epoch. See Fig. 2. The results in this report use single-frequency pseudorange and Doppler measurements achieving mean horizontal positioning accuracy of 0.70 m for the PPP INS algorithm for both the consumer grade (CG) or navigation grade (NG) sensors. The NG-INS and CG-INS algorithms achieve

horizontal position error ≤ 1.5 m at 95.9% and 95.0%, respectively; and, vertical position error ≤ 3 m at 70.4% and 69.2%, respectively. Both surpass the SAE specification.

This study focuses on single frequency, single constellation (i.e. GPS only) results. The performance was heavily dependent upon the number of measurements (i.e., satellite signals) available. See Fig. 3. The upcoming availability of multiple constellations (i.e., GPS, Biedou, Galileo, Glonass) will greatly increase the number of available measurements. The increased number of signal frequencies will facilitate estimation of ionospheric delay. The combined increase in number of measurements across constellations and frequencies will facilitate accommodation of outliers, accommodation of multipath, and enhance the geometric diversity (i.e., GDOP) of the solutions which will combine to enhance the reliability of achieving the performance specification.

II. POSITION ESTIMATION ALGORITHMS

The experimental results in Section III will consider the performance of three estimation approaches using data from a moving platform. All three approaches use the PPP corrections described in eqn. (7) in [12].

1) PPP-LS: This algorithm uses least squares (LS). When there are five or more satellites, the state vector is defined as

$$\mathbf{x}(t) = [\mathbf{p}^T, t_r, \delta A_v]^T \in \Re^5$$

where $\mathbf{p} \in \mathbb{R}^3$, $t_r \in \mathbb{R}^1$ and $\delta A_v \in \mathbb{R}^1$ denote rover position, receiver clock bias and residual vertical atmospheric delay, respectively. In the case of 4 satellites, the residual atmospheric delay state δA_v is dropped to enable a solution. If there are less than 4 satellites, no solution is possible. At each GPS epoch, the GPS L1 PPP corrected pseudorange measurement equation is solved for the optimal state estimate independent of any prior information. This requires at least $m = 5$ measurements at each time step. These estimates are point-wise, without any filtering.

The PPP-LS approach is included mainly because its a posteriori residuals (i.e., model misfit) at each epoch provide a useful indicator of the measurement quality at that epoch.

2) Navigation-Grade (NG) PPP-INS: This algorithm implements a PPP GPS aided inertial navigation system using a navigation-grade inertial measurement unit (NV-IMU 1000). The state vector is

$$\mathbf{x}(t) = [\mathbf{p}^T, \mathbf{v}^T, \mathbf{q}^T, \mathbf{b}_a^T, \mathbf{b}_g^T, \delta A_v]^T \in \Re^{17}$$

The symbols $\mathbf{p}, \mathbf{v}, \mathbf{b}_a, \mathbf{b}_g \in \mathbb{R}^3$ represent the position, velocity, accelerometer bias and gyro bias vectors, $\mathbf{q} \in \mathbb{R}^4$ represents the attitude quaternion, and $\delta A_v \in \mathbb{R}^1$ represents residual vertical atmospheric delay. The state is integrated through time using the IMU data and corrected using an extended Kalman Filter (EKF). The aiding measurements are the single-differenced (between satellites) L1 Doppler and PPP corrected pseudorange measurements.

3) Consumer-Grade (CG) PPP-INS: This algorithm is exactly the same as that described for the NG PPP-INS. The IMU

data for this implementation is from the NV-IMU 1000, but artificially corrupted to have the characteristics of a consumer-grade IMU (i.e., ADIS16360) (see the appendix of [11]).

Each algorithm processes the same set of GNSS measurements ($k = 1, \ldots, N_d$). Processing is incremental, as if they were occurring in real-time (i.e., to estimate the state $x(t)$ only the GPS and IMU measurements prior to time t are used in the computation). The details of the algorithms are discussed further in [8].

III. EXPERIMENTAL RESULTS

The goal of this section is to analyze the ability to achieve either SAE specification [7] or a one-meter horizontal positioning accuracy specification for moving platforms using L1 PPP GPS data. The PPP approach is described in [12]. The estimation algorithms are summarized in Section II.

A. Data Acquisition

During data acquisition, the hardware was mounted on a sedan that was driven repeatedly along a multi-block section of an urban street (Columbia Ave. near the intersection with Iowa Avenue in Riverside, CA) with low buildings and trees adjacent to the street. That section of street has two stop lights. The trajectory involves two U-turns, one at each end. Therefore, the trajectory includes acceleration, deceleration and turn rates typical for urban trajectories. The experiment lasted 1000 seconds. The experimental data were saved for post-processing so that algorithmic analysis could be performed. All state estimation results were produced using only pseudorange and Doppler data available prior to the time of the state estimate calculation (i.e., filtering, not smoothing). Phase measurements were not used for state estimation, because integer ambiguity resolution is not reliable in real-time for single-frequency GPS receivers, especially with small numbers of satellites.

The PPP information to compensate the common-mode errors was collected from external sources [12]. The satellite orbit, clock and hardware bias model parameters were collected from IGS-RTS using the BNC software. The ionospheric delay model parameters were obtained from US-TEC real-time data. Tropospheric error was corrected using the UNB3M model for an approximate user-location.

The on-vehicle experimental hardware included two GNSS receivers and one IMU. One receiver was a single frequency u-Blox ZED-F9P (consumer grade) and the other was a dual frequency NOVATEL OEMV2 (survey grade). Both receivers were connected to the same Antcomm ANN-MS-0-005 antenna. The ZED-F9P single-frequency receiver provided GNSS data for state estimation for the LS and INS approaches.

The INS implementation also used inertial measurement data. The IMU on the vehicle was an NV-IMU 1000, which was a navigation-grade sensor. To analyze navigation performance for a consumer-grade IMU the NV-IMU 1000 data was corrupted with additive stochastic errors corresponding to the specification of the ADIS16360 IMU from Analog Device. The stochastic error generation methodology is described in the Appendix of [11].

B. Accuracy Metric

One of the metrics for comparison of algorithms will be the norm of the horizontal position error at time k. This metric is computed as

$$e_{h_k}^a = \left\| \begin{bmatrix} 1 & 0 & 0 \\ 0 & 1 & 0 \end{bmatrix} (\mathbf{p}_r - \hat{\mathbf{p}}_k^a) \right\|. \qquad (1)$$

This equation assumes that the position vector is represented in the North-East-Down navigation frame. The symbol $\hat{\mathbf{p}}_k^a$ denotes the position estimated at time k and for algorithm $a \in \{1, 2, 3\}$. The three algorithms are defined in Section II with results summarized in Tables I and II. The symbol $\mathbf{p}_r$ is the receiver antenna's ground truth position, as discussed in Section III-C.

C. Ground Truth Trajectory

Ground truth trajectory estimation was performed in post-processing using a Maximum a Posteriori smoothing algorithm [13]. It used the two-frequency pseudorange and integer-resolved, carrier phase GNSS data from the OEMV2 and NV-IMU 1000 to achieve centimeter accuracy. This ground truth trajectory and OEMV2 data are only used to assess the accuracy of the state estimation results using eqn. (1). OEMV2 data is not used in state estimation.

D. Data Quality Metrics

For state estimation by any algorithm, an important item to consider is the quality of the available data. For GNSS data, a few factors to consider are the number of satellites, the geometry of the satellites, and the accuracy of the range measurements due to local factors (multipath, foilage, etc.)

Geometric Dilution of Precision (GDOP) quantifies the geometry of the user-to-satellite direction vectors for the available satellites at time instant k. GDOP is computed as

$$GDOP(k) = \sqrt{trace(H_k^T H_k)^{-1}} \qquad (2)$$

where H_k is the observation matrix constructed by stacking the user-to-satellite direction vectors. Higher GDOP values indicate worse geometric diversity which leads to a larger position error covariance matrix.

One indicator of the quality of a set of m measurements is the risk r_k that is computed as

$$r_k = \frac{1}{m} \sum_{i=1}^{m} |r_k^i|. \qquad (3)$$

The symbol m indicates the number of available satellites at time epoch k. In this expression, r_k^i is the posterior measurement residual for the ith satellite after convergence of the nonlinear least squares estimation process. Each $|r_k^i|$ indicates the degree to which that measurement conformed to the measurement model, given the full set of measurements.
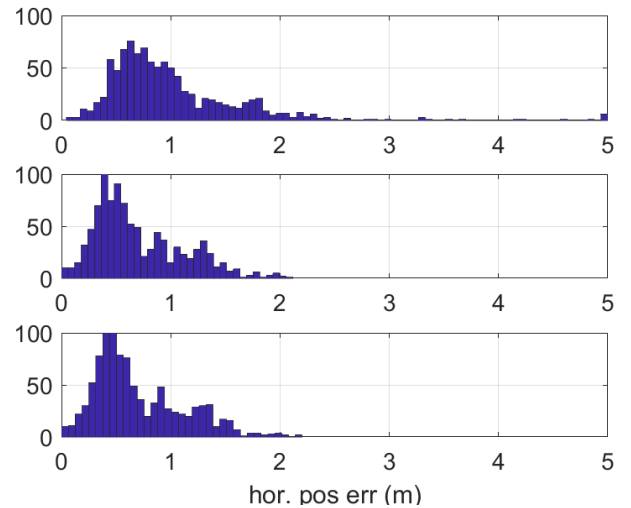

Fig. 1: Histogram of horizontal position error $e_{h_k}^a$ defined in eqn. (1) for LS algorithm (Top), NG-INS algorithm (Middle) and CG-INS algorithm (Bottom).

E. Positioning Performance

Fig. 1 shows histograms of $e_{h_k}^a$ as defined in eqn. (1). The top figure is for LS, the middle one is for NG-INS and the bottom one is for CG-INS. The plot is generated using $N_d = 1000$ epochs. Each algorithm uses the same GNSS dataset. For construction of the histogram, all epochs for which $e_{h_k} >= 5$ are placed into the bin that includes $e_{h_k} = 5$.

Tables I and II summarize various measures of positioning accuracy for horizontal (e_{h_k}) and vertical positioning (e_{v_k}), respectively. Column 1 shows name of the algorithm corresponding to that row. Column 2 displays the mean position error. Column 3 contains the standard deviation of the position error. Column 4 shows the maximum value of the position error. Columns 5 and 6 report the percentage of samples that have a positioning error less than the accuracy specified in the column header.

The result shows that both INS algorithms and the LS horizontal accuracy satisfy the SAE J2945 specification (horizontal error ≤ 1.5 m and vertical error ≤ 3 m 68%), but the LS vertical

Algorithm	Mean	Std. Dev	Max	Prob. of $e_{h_k}^a$		
				$< 1m$	$< 1.5m$	$< 2m$
1. LS	1.01	0.65	9.35	63.1	83.1	94.2
2. NG-INS	0.70	0.41	2.11	76.9	95.9	99.7
3. CG-INS	0.71	0.40	2.20	76.7	95.0	99.5

TABLE I: Horizontal Error Statistics.

Scenario	Mean	Std. Dev	Max	Prob.	
				$e_{v_k}^a < 2m$	$e_{v_k}^a < 3m$
1. LS	3.57	3.14	13.12	40.3	56.2
2. NG-INS	2.50	0.96	4.5	45.2	70.4
3. CG-INS	2.52	0.96	4.56	44.3	69.2

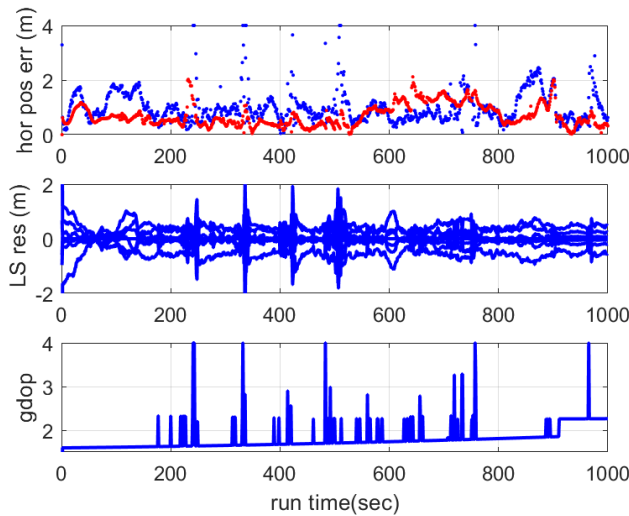TABLE II: Vertical Error Statistics.

Fig. 2: Performance and data quality metrics. Top - Horizontal position error computed by eqn. (1) for LS and CG-INS. Middle - LS Measurement residual. Bottom - GDOP.

Fig. 3: Mean and standard deviation of horizontal position error vs number of available satellites m for LS (blue line with red dots) and CG-INS (green line with black dots)

position fails to achieve the specification.

The performance of NG-INS and CG-INS is similar for this particular dataset and the one-second epoch period. The performance difference between NG-INS and CG-INS would become more apparent for larger epoch periods or in situations where GNSS measurement became unavailable for longer periods of time (10s of seconds). This discussion is out of scope for this report.

F. Performance Analysis

The section discusses the characteristics of the dataset as they relate to the performance of each algorithm.

The top row of Fig. 2 shows the horizontal position error data versus time for LS (blue) and CG-INS (red). The horizontal position error axis limit is 4 m to provide higher resolution to the curves below that magnitude. Time epochs at which $e_{h_k} >= 4$ are indicated by a dot on the axis limit (i.e., 4 m). The measurement residual for the LS algorithm is in the middle. GDOP is displayed on the bottom row.

The GDOP plot indicates that (1) the geometry of the set of available satellites generally gets worse (increasing from below to above 2) over the period of the experiment, and (2) the geometry deteriorates or improves at certain epochs as satellites are blocked or unblocked. The LS residual plot shows that in addition to satellite geometric considerations, local conditions (e.g., foilage, multipath) can also affect the accuracy of the measurements themselves, even at epochs ($t < 200s$) when the geometry is good.

Fig. 2 shows that the LS algorithm is more affected by the PPP GPS signal availability and measurement quality issues than the CG-INS algorithm. There are two dominant reasons for this. First, the INS approaches have more data because they use the IMU data as well as the PPP GPS data. Second, the LS approach has no filtering. Each epoch is solved using only the
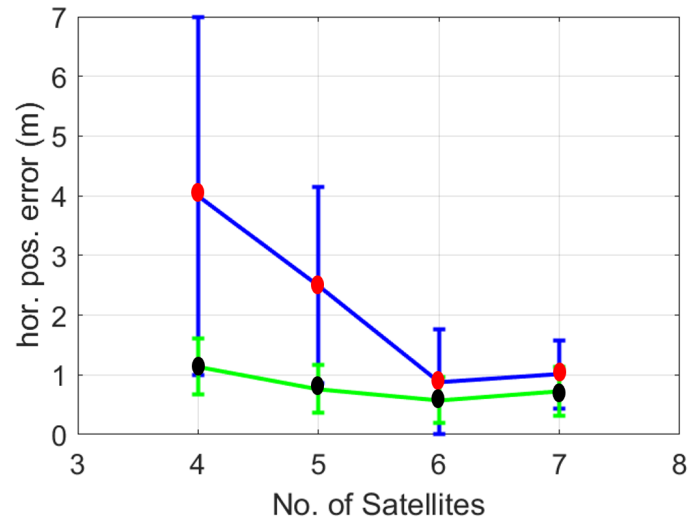
PPP GPS measurements available at that epoch. The CG and NG INS approaches use the IMU data and filtered effects (achieved through an extended Kalman filter) of all previous PPP-GPS epochs to estimate the state at the current epoch. Therefore, the CG-INS approach is less affected by short time durations with few measurements, poor geometry of available measurements, or unreliable residuals.

Another aspect affecting performance is illustrated in Fig. 3, which shows horizontal error statistics as a function of the available number of measurements m for both LS and CG-INS. The red points connected by a blue line correspond to the mean of the LS error. The blue vertical bar shows the corresponding error standard deviation. The black points connected by a green line correspond to the mean of the CG-INS error. The green vertical bar shows the corresponding error standard deviation. To produce this figure, for $m = 4$, the time epochs where the horizontal position error was larger than 4 were discarded from LS. Inclusion of those epochs would only strengthen the conclusions, but would expand the magnitude of the y-axis, making its resolution worse. Discarding these epochs, yields a LS mean position error of 4 m. For LS, sub-meter accuracy is achieved for $m \geq 6$. For INS, the average position error is sub-meter for $m > 4$. Performance tends to improve as the number of available measurements increases.

These results do not incorporate any methods to accommodate outlier measurements. As the number of measurements increases, the effectiveness of outlier accomodation increases, as these methods have more measurements from which to select.

Corresponding to the SAE spec for horizontal positioning accuracy at 2 m, in the 1000 seconds dataset, there are 56 seconds with position error exceeding 2 m. Among these 56 epochs, 41 of them have risk factor ≥ 1 m and 8 epochs have GDOP value exceeding 2.3. Thus poor geometric diversity (high

GDOP) and high risk measurements are main reasons causing the LS estimation algorithm to have positioning accuracy exceeding 2 m. These same factors adversely affect the PPP GPS aided INS accuracy. The growing number of GNSS constellations will greatly increase satellite geometric diversity, reducing GDOP. Both the growing number of frequencies and constellations will enhance the number of measurements to select from to achieve a usable measurement set with low risk.

IV. CONCLUSIONS

The Phase C report [12] discussed the GNSS measurement model, common-mode errors, real-time WADGNSS correction services, common-mode error computation methods using these services, description of the implementation of real-time PPP using single frequency pseudorange and Doppler measurements, and demonstrated sub-meter positioning performance for stationary receivers. This report extends that experimental study to the dynamic environment of a moving platform.

The dataset for this study used a single-frequency consumer grade GPS receiver that only received signals from the GPS constellation. The maximum number of available available measurements was 7. All algorithms herein used all the available measurements, without outlier accommodation. Under these circumstances LS achieved mean horizontal position error of 1.01 m with standard deviation of 0.65 m. The horizontal position achieved 1.0 m accuracy at 63.1% and 2 m accuracy at 94.2%. The vertical position achieved 3.0 m accuracy at 56.2%. The horizontal performance achieved the SAE specification, while the vertical performance did not. The LS algorithm was mainly included to provide a posteriori residuals to enable discussion of outlier risk. The LS performance could be improved by various filtering approaches such as Kalman filtering with a position, velocity, acceleration model see [9], [11]. INS algorithm achieves mean horizontal position error of 0.70 m with standard deviation of 0.65 m. The horizontal position achieved 1.0 m accuracy at 76.7% and 2 m accuracy at 95.0%. The vertical position achieved

3.0 m accuracy at 69.2%. This performance surpasses the SAE specification.

Incorporation of other GNSS constellations (GLONASS, Beidou, GALILEO) along with robust outlier detection algorithm will improve the positioning performance. Implementation of PPP for multi-GNSS system and the utilization of various measurement selection algorithms are two important future research topics.

V. ACKNOWLEDGEMENT

[1] Z. Wang, Y. Bian, S. Shladover, G. Wu, S. Li, and M. Barth, "A survey on cooperative longitudinal motion control of multiple connected and automated vehicles," *IEEE Intelligent Transportation Systems Magazine*, pp. 4–24, 2020.

[2] J. A. Farrell, T. D. Givargis, and M. J. Barth, "Real-time differential carrier phase GPS-aided INS," *IEEE Transactions on Control Systems Technology*, vol. 8(4), pp. 709–721, 2000.

[3] P. Teunissen, "Differential GPS: Concepts and Quality Control," *Netherlands Institution of Navigation, Amsterdam*, 1991.

[4] P. K. Enge, R. M. Kalafus, and M. F. Ruane, "Differential operation of the global positioning system," *IEEE Comm. Mag.*, vol. 26(7), pp. 48–60, 1988.

[5] C. Shuxin, Y. Wang, and C. Fei, "A study of differential GNSS positioning accuracy," *3rd Int. Conf. on Microwave and Millimeter Wave Tech.*, pp. 361–364, 2002.

[6] P. Misra and P. Enge, *Global Positioning System: Signals, Measurements and Performance*. Massachusetts: Ganga-Jamuna Press, 2 ed., 2006.

[7] Anonymous, "On-Board System Requirements for V2V Safety Communications," tech. rep., Society of Automotive Engineers, March, 2016.

[8] F. Rahman, E. Aghapour, and J. A. Farrell, "ECEF Position Accuracy and Reliability in the Presence of Differential Correction Latency: Phase A Technical Report," tech. rep., University of California, Riverside (escholarship.org/uc/item/38d3h08w), October, 2018.

[9] F. Rahman, E. Aghapour, and J. A. Farrell, "ECEF Position Accuracy and Reliability in the Presence of Differential Correction Latency," *IEEE/ION PLANS*, pp. 583–588, 2018.

[10] E. Aghapour, F. Rahman, and J. A. Farrell, "Risk-averse performance-specified state estimation," *IEEE/ION PLANS*, pp. 627–633, 2018.

[11] F. Rahman and J. A. Farrell, "ECEF Position Accuracy and Reliability in the Presence of Differential Correction Latency: Phase B Technical Report," tech. rep., University of California, Riverside (escholarship.org/uc/item/135578mw), June, 2019.

[12] F. Rahman and J. A. Farrell, "ECEF Position Accuracy and Reliability:Continent Scale Differential GNSS Approaches: Phase C Technical Report for Sirius XM," tech. rep., University of California, Riverside (https://escholarship.org/uc/item/05p9p3c9), July, 2019.

[13] A. Vu, J. A. Farrell, and M. Barth, "Centimeter-accuracy smoothed vehicle trajectory estimation," *IEEE Intel. Transp. Sys. Mag.*, vol. 5(4), pp. 121–135, 2013.